PHYSICAL REVIEW B VOLUME 20, NUMBER 8 15 OCTOBER 1979

Electronic structure of Ni_3Ti

T. E. Fischer and S. R. Kelemen
Exxon Research and Engineering Company, P.O. Box 45, Linden, New Jersey 07036

K. P. Wang* and K. H. Johnson
Department of Materials Science and Engineering, Massachusetts Institute of Technology, Cambridge, Massachusetts 02139

(Received 30 May 1979)

The electronic structure of the intermetallic compound Ni_3Ti was investigated theoretically with self-consistent-field (SCF)-$X\alpha$ calculations on the appropriate four-atom tetrahedral cluster. The calculations show a d band consisting of filled Ni d orbitals, empty Ti d orbitals, and half-filled Ni-Ti antibonding orbitals near the Fermi level. We obtain from the calculations a charge transfer from Ti to Ni and to the interatomic space so that ionic and covalent components are added to the metallic bond. The energy distributions of photoelectrons from the polycrystalline compound Ni_3Ti were obtained at $h\nu = 11.7$, 16.8, 21.2, 26.8, and 40.8 eV and reproduce the features of the calculated electronic structure, namely, a relatively low density of states at the Fermi level and a bandwidth of 3 eV. The Auger peaks of nickel and titanium were obtained at the same energies as for the elemental metals and are in agreement with the theoretical finding that the core levels in the compound are at the same energies as in the elements.

I. INTRODUCTION

The nickel-titanium alloy systems possess a number of interesting mechanical and chemical properties.[1] Some of these properties, such as "shape memory",[2] hydrogen storage,[3] the formation of compounds with large negative energies of formation,[4] and the chemical properties of their surfaces have their origin in the nature of the intermetallic bond and thus in the energies and shapes of the valence-electron orbitals. It is useful to probe the electronic structures of these alloys experimentally and theoretically.

In this paper we report on photoemission, work function, and Auger spectroscopy on Ni_3Ti and on theoretical studies of the electronic structure of this compound. A comparison of this electronic structure with that of pure nickel will serve as a basis for speculating on the chemical properties of its surface.

Our knowledge of the electronic structure of alloys, particularly transition-metal alloys, is still in a rudimentary stage when compared to that of pure metals. In the dilute limit, the electronic structure of transition-metal alloys can be generally understood in terms of the Friedel-Anderson virtual-impurity-state concept[5] or more recent self-consistent-field cluster molecular orbitals.[6] But for the more concentrated cases, we are still lacking reliable quantitative theoretical methods. One of the difficulties is that alloys are often in a disordered state and a careful configuration average is required. The best approximate methods[7] such as the average-t-matrix method, the coherent-potential approximation, all based on the reciprocal or k-space representation and multiple-scattering theory, often give results which are not in satisfactory agreement with experiment.[8] Even in the case of ordered alloys such as Ni_3Ti, one still has to face the important problem of charging effects.[9] It is well known that "charge transfer" is a very important factor in understanding the electronic properties of alloys. It affects important properties of the metal, such as its brittleness or the chemical reactivity of its surface. Charge transfer affects the electrical potential contributed by a given component of the alloy. Since this potential determines the electron wave functions and hence the distribution of electric charge, a self-consistent calculation is obviously required. Because of the complexity of such calculations, conventional methods, based on the k-space representation, are generally inadequate to handle this charging problem.

Recent work on the electronic structure of metal clusters[10] calculated by the self-consistent-field $X\alpha$ scattered-wave (SCF-$X\alpha$-SW) method[11] shows that by a proper choice of size and configuration, the clusters mimic with remarkable accuracy key features of the bulk band structures and local densities of states. This theoretical approach has been extended recently to the problems of dilute transition-metal alloy electronic structure, local magnetic moments, and the Kondo effect.[6] These results suggest the further extension of this technique to nondilute alloys. The most important advantage of adapting the SCF-$X\alpha$-SW cluster molecular-orbital method to nondilute alloys is that charging effects can be handled straightforwardly in direct, rather than reciprocal, space.

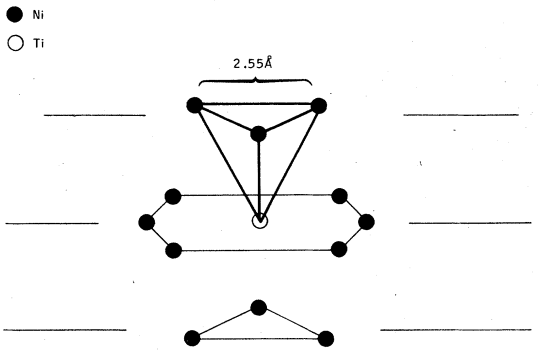

FIG. 1. Spacial positions of Ni and Ti atoms in a Ni_3Ti crystal (Ref. 12–14). The four-atom Ni_3Ti tetrahedron is shown.

In the cluster representation of a nondilute alloy, the most crucial step is to choose a proper cluster configuration which is large enough to simulate the mean local environment experienced by the electron, yet small enough to minimize the problem of configuration averages. In our work, we have taken from crystallographic data[12-14] a four-atom tetrahedron containing three nickel atoms and one titanium atom and possessing C_{3v} symmetry as the cluster simulating the local environment of Ni_3Ti (Fig. 1). As a reference point for the effects of alloying, we have also calculated the electronic structure of a four-atom tetrahedral cluster of T_d symmetry representing pure fcc nickel.

The cluster calculations are compared to the results of our spectroscopy measurements and those of other experiments in order to understand the electronic structure of this compound.

II. EXPERIMENTAL TECHNIQUES

The sample of the intermetallic compound Ni_3Ti was prepared from Marz-grade nickel and titanium foils obtained from Materials Research Corp. The sample was prepared by arc melting weighed amounts of the starting materials in an argon atmosphere. Homogeneity of the alloy was assured by repeated stirring and arc melting. The intermetallic compound Ni_3Ti was arc cut and mechanically polished before insertion into the vacuum chamber.

The alloy contained significant amounts of sulfur, phosphorus, and oxygen impurities. The sample underwent extensive cleaning treatments which consisted of sputtering with argon ions at various sample temperatures up to 1000°C during a cumulative time of approximately 50 h. This procedure ensured segregation to the surface of the impurities and their removal by ion bombardment. After this treatment no surface impurities were detected with Auger electron spectroscopy. The surface of the sample then remained free of impurities after annealing in vacuum at 1000°C for 5 min.

Ultraviolet photoemission spectroscopy (UPS) was performed in the usual manner by measuring the energy distribution of electrons emitted by the samples under irradiation with ultraviolet light from a differentially pumped rare-gas resonance lamp. The energy distributions of the electrons were measured with a double-pass cylindrical mirror analyzer (Physical Electronics).

III. EXPERIMENTAL RESULTS

A. Ultraviolet photoemission spectroscopy

Figure 2 shows the results of the measurements obtained with photon energies $h\nu = 40.8$, 21.2, 16.8, and 11.7 eV. Energy distributions of photoelectrons such as those of Fig. 2 are the result of the excitation of electrons from the valence bands of the material into a higher conduction band and their escape into vacuum. They represent the density of states in the valence band modulated by the probability of photoexcitation, the energy-dependent density of states in the conduction band and the probability of escape into vacuum. All these modulating quantities vary with the photon energy of the ultraviolet light; consequently, features of the energy distributions which are common to all the

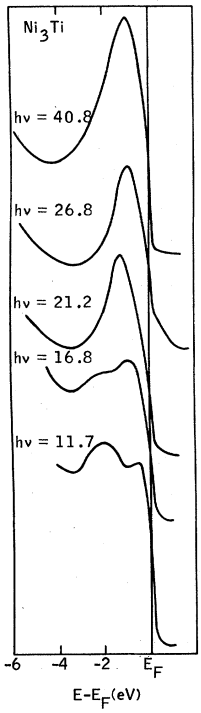

FIG. 2. Energy distributions from photoelectrons from Ni_3Ti. Photon energies are as labeled.

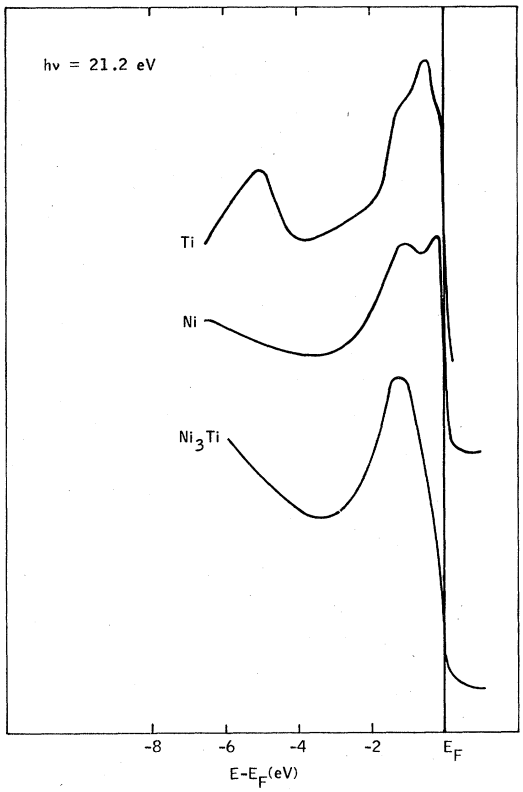

FIG. 3. Comparison of energy distributions of photoelectrons at $h\nu = 21.2$ eV from Ni_3Ti, nickel (Ref. 17), and titanium (Ref. 15).

employed exciting photon energies can be attributed with some confidence to features in the electronic structure of the valence band of the material. Figure 3 shows the energy distribution from Ni_3Ti at $h\nu = 21.2$ and for comparison the energy distributions for pure nickel and titanium published by Eastman.[15,17] The energy distributions of Fig. 3 show that the electronic structure of the nickel-titanium alloys cannot be considered as a combination, (superposition or average), of the densities of states of pure nickel and titanium. Alloying forms a new electronic structure which is characterized by a relatively low density of states near the Fermi level. The work function of Ni_3Ti is 4.5 eV as obtained from the photoemission energy distributions. This value is lower than that observed on any of the low-index faces of Ni whose values are between 0.2 and 0.8 eV higher. In the following sections, these experimental results will be compared with calculations of the electronic structure.

B. Auger electron spectroscopy

We have examined the position and shape of the *LMM*, *LMV* and *LVV* Auger electron peaks of titanium and nickel in the alloy for experimental evidence of core level shifts and other changes in electronic structure that result from alloy formation. Within the accuracy of our experiments (±1 eV) the absolute energies of the peaks in their differential or direct form are the same as for the elemental metals. A more accurate measure can be obtained from the energy differences between the three Auger peaks. These are again the same as for the elements. In case of a chemical shift Δ of the effective ionization energies of the L_{23} and M_{23} levels, one would expect the *LMM* peak to shift by $-\Delta$, the *LMV* peak to remain constant, and the *LVV* peak to shift by $+\Delta$. The comparison of peak spacing thus indicates no shift ($|\Delta| < 0.1$ eV) of the core levels of Ti or Ni.

IV. CALCULATIONS

We have performed self-consistent-field $X\alpha$ molecular-orbital calculations of tetrahedral clusters, consisting of four nickel atoms (Ni_4), and another containing three nickel atoms and one titanium atom (Ni_3Ti). The interatomic distances chosen for the Ni_4 cluster are the same as in bulk fcc nickel; in the Ni_3Ti cluster they were chosen equal to those in the crystalline Ni_3Ti compound which forms the hexagonal $D0_{24}$ prototype.[12-14] The cluster structures thus represent the short-range

TABLE I. Parameters used in the SCF-$X\alpha$-SW calculations for Ni_4 and Ni_3Ti clusters.

	Ni_4	Ni_3Ti	
α [a]	0.709	0.709 (Ni)	0.717 (Ti)
Internuclear distance (a.u.)	4.71	4.82 (Ni-Ni)	4.81 (Ni-Ti)
Atomic sphere radius (a.u.)	2.35	2.41 (Ni)	2.43 (Ti)
Outer sphere radius (a.u.)	5.23	5.36	

[a]These are the exchange-correlation parameters for the component atoms determined by matching the $X\alpha$ total energy of the atom to the Hartree-Fock total energy, as described in Ref. 11. In the intersphere region, the α value is taken as a weighted mean of the component values.

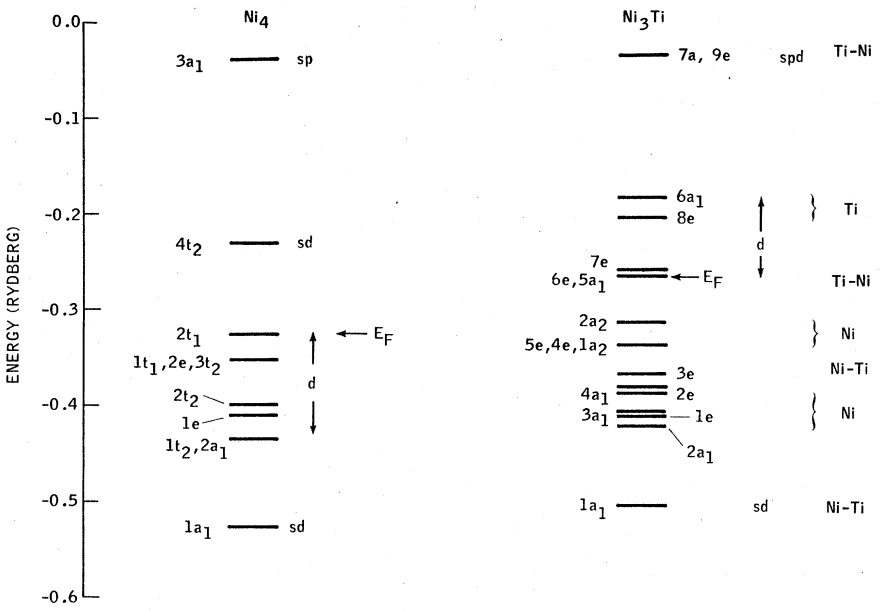

FIG. 4. Spin-restricted electronic energy levels for a tetrahedral Ni_4 cluster (left-hand side) and a tetrahedral Ni_3Ti (right-hand side), as calculated by the SCF-$\chi\alpha$-SW method.

order of the corresponding bulk materials. The important parameters used in the calculations are listed in Table I.

The calculations for Ni_4 will be compared to the density of states of bulk nickel to verify the suitability of this simple model material. Then a comparison of the Ni_4 and Ni_3Ti calculations will be made to describe the electronic effects of alloying.

A. Ni_4

The spin-restricted molecular-orbital energies for the Ni_4 cluster are displayed on the left-hand side of Fig. 4 with the levels labeled according to the irreducible representations of the T_d point group and principal partial-wave character. The core levels not shown in the figure are listed separately in Table II. The levels in the energy range between −0.43 and −0.32 Ry correspond to predominantly d-like orbitals, whereas $1a_1$ (−0.528) and $4t_2$ (−0.230) levels correspond to s-like orbitals with substantial d admixture. The "Fermi level" E_F, designates the highest occupied spin orbital $2t_1$ (−0.32) and is filled only partially with four electrons. By applying Hund's rules to the orbital occupation in Ni_4, one finds that there are unpaired spins, leading to a net spin polarization and "paramagnetism" of the cluster.

Since Ni_4 is paramagnetic, a more accurate representation of the electronic structure can be obtained by carrying out a spin-polarized molecular-orbital calculation.[6] The results of such a calculation are shown on the left-hand side of Fig. 5. It can be seen from Table III where we list energies, occupancies, charge distributions, and fractional principal partial-wave character of all occupied orbitals of Ni_4, that the levels in the energy range between −0.43 and −0.30 Ry correspond to predominantly d-like orbitals (they can be considered as the counterpart of the d bands in bulk nickel), whereas the $1a_1$ and $4t_2$ levels correspond predominantly to s-like orbitals (and can be considered analogous to the overlapping s band in bulk nickel) with substantial d admixture. An analysis of the computed wave functions indicates that most of the orbitals near the top of the d band are antibonding or nonbonding while most of the orbitals near the bottom of the d band are bonding. We illustrate this by presenting the contour maps for $2t_1\uparrow$ and $1a_1\uparrow$ states plotted in the (100) plane containing two Ni atoms, in Figs. 6 and 7, respec-

TABLE II. Energy of Ni core levels of Ni_4 and Ni_3Ti as calculated by the spin-polarized SCF-$X\alpha$-SW method. Energies are in rydbergs.

	Ni_4	Ni_3Ti
$1S\uparrow$	−596.19	−596.21
$1S\downarrow$	−596.19	−596.21
$2S\uparrow$	−70.33	−70.34
$2S\downarrow$	−70.33	−70.33
$3S\uparrow$	−7.52	−7.53
$3S\downarrow$	−7.51	−7.50
$2P\uparrow$	−61.46	−61.48
$2P\downarrow$	−61.46	−61.46
$3P\uparrow$	−4.81	−4.82
$3P\downarrow$	−4.81	−4.79

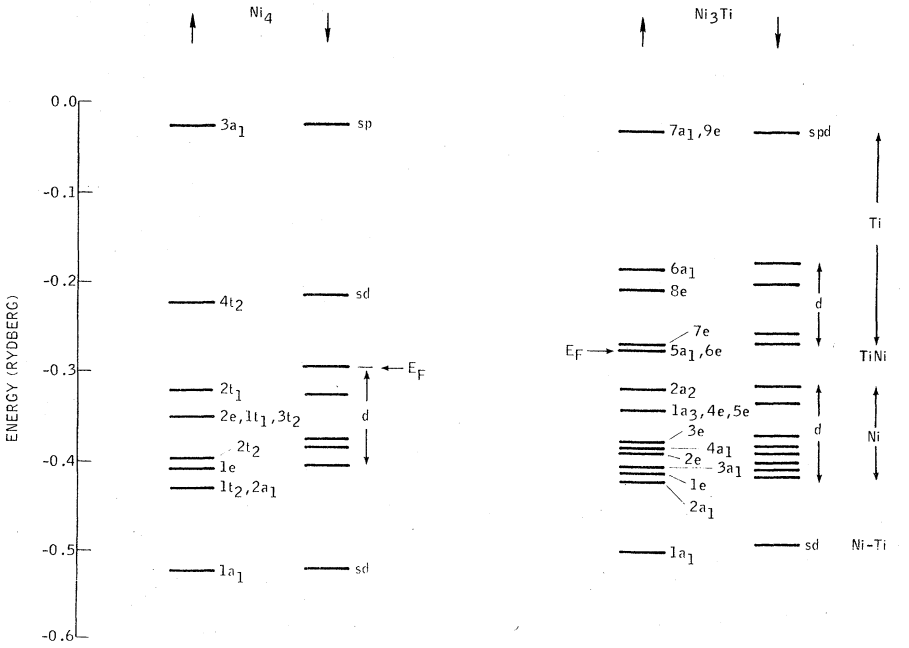

FIG. 5. Spin-polarized electronic energy levels for a tetrahedral Ni_4 cluster (left-hand side) and a tetrahedral Ni_3Ti (right-hand side), as calculated by the SCF-$\chi\alpha$-SW method.

TABLE III. Energies, occupancies, charge distributions, and fractional principal partial-wave character for the occupied molecular orbitals of a tetrahedral Ni_4 cluster, as determined by the spin-polarized SCF-$X\alpha$-SW method. Orbital energies are in rydbergs. Occupancies and charges are in electrons. Q(inter) is the intersphere charge. Q(extra) is the extramolecular charge. Q(Ni) is the Ni sphere charge. Total Q(Ni)↑: 13.771; total Q(extra)↑: 0.293; total Q(inter)↑: 1.625; total Q(Ni)↓: 13.258; total Q(extra)↓: 0.296; total Q(inter)↓: 1.671.

Orbital (occupancy)	Energy	Q(Ni)	(Principal partial-wave components)	Q(extra)	(Principal partial-wave components)	Q(inter)
$3a_1$↑(0)	−0.029	3.93×10^{-2}	[0.079(s), 0.770(p) 0.151(d)]	75.93×10^{-2}	[0.986(s)]	8.34×10^{-2}
$3a_1$↓(0)	−0.027	3.77×10^{-2}	[0.084(s), 0.753(p) 0.163(d)]	77.90×10^{-2}	[0.986(s)]	7.84×10^{-2}
$4t_2$↑(0)	−0.220	10.07×10^{-2}	[0.410(s), 0.402(d)]	28.40×10^{-2}	[0.994(p)]	31.28×10^{-2}
$4t_2$↓(0)	−0.212	10.50×10^{-2}	[0.359(s), 0.468(d)]	28.52×10^{-2}	[0.478(p)]	29.47×10^{-2}
$2t_1$↑(3)	−0.320	23.89×10^{-2}	[0.992(d)]	1.51×10^{-2}	[0.863(f), 0.137(g)]	2.91×10^{-2}
$2t_1$↓(1)	−0.295	23.82×10^{-2}	[0.992(d)]	1.66×10^{-2}	[0.866(f), 0.134(g)]	3.08×10^{-2}
$1t_1$↑(3)	−0.349	24.03×10^{-2}	[1.000(d)]	0.33×10^{-2}	[0.986(g)]	3.55×10^{-2}
$1t_1$↓(3)	−0.324	23.98×10^{-2}	[1.000(d)]	0.36×10^{-2}	[0.983(g)]	3.70×10^{-2}
$3t_2$↑(3)	−0.349	22.95×10^{-2}	[0.981(d)]	1.32×10^{-2}	[0.455(p), 0.260(d)]	6.89×10^{-2}
$3t_2$↓(3)	−0.326	22.62×10^{-2}	[0.978(d)]	0.17×10^{-2}	[0.549(p), 0.235(d)]	7.84×10^{-2}
$2e$↑(2)	−0.350	23.61×10^{-2}	[0.997(d)]	1.23×10^{-2}	[0.975(d)]	4.35×10^{-2}
$2e$↓(3)	−0.326	23.48×10^{-2}	[0.996(d)]	1.42×10^{-2}	[0.978(d)]	4.64×10^{-2}
$2t_2$↑(3)	−0.395	22.67×10^{-2}	[0.984(d)]	1.19×10^{-2}	[0.101(p), 0.447(d) 0.412(f)]	8.12×10^{-2}
$2t_2$↓(3)	−0.373	22.49×10^{-2}	[0.983(d)]	1.37×10^{-2}	[0.121(p) 0.407(f), 0.438(d)]	8.67×10^{-2}
$1e$↑(2)	−0.404	23.60×10^{-2}	[0.995(d)]	0.45×10^{-2}	[0.492(g)]	5.14×10^{-2}
$1e$↓(2)	−0.380	23.53×10^{-2}	[0.994(d)]	0.48×10^{-2}	[0.997(g)]	5.39×10^{-2}
$2a_1$↑(1)	−0.427	19.34×10^{-2}	[0.923(d)]	4.13×10^{-2}	[0.863(s)]	18.31×10^{-2}
$2a_1$↑(1)	−0.408	19.87×10^{-2}	[0.947(d)]	3.87×10^{-2}	[0.832(s)]	16.66×10^{-2}
$1t_2$↑(3)	−0.427	22.20×10^{-2}	[0.936(d)]	1.00×10^{-2}	[0.118(d), 0.476(p) 0.225(f)]	10.21×10^{-2}
$1t_2$↓(3)	−0.406	21.84×10^{-2}	[0.924(d)]	1.24×10^{-2}	[0.565(p), 0.101(d) 0.182(f), 0.154(g)]	11.41×10^{-2}
$1a_1$↑	−0.521	16.04×10^{-2}	[0.628(s), 0.272(d)]	5.73×10^{-2}	[0.953(s)]	30.12×10^{-2}
$1a_1$↓	−0.512	15.33×10^{-2}	[0.677(s), 0.213(d)]	6.29×10^{-2}	[0.964(s)]	32.38×10^{-2}

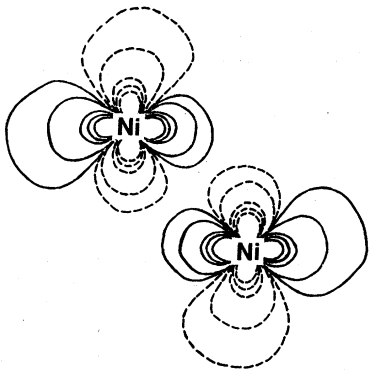

FIG. 6. Contour maps for the highest occupied orbital $2t_1$, in the tetrahedral Ni_4 cluster, plotted in a plane containing two Ni atoms. Contour values decrease in absolute value with decreasing absolute values of the contour labels, the sign of the label giving the sign of the wave function. The zero contour indicates a mode on the wave function.

tively. It is clearly seen that $2t_1\uparrow$ is an antibonding d-like orbital whereas $1a_1\uparrow$ is a bonding s-d hybrid orbital. Because of the more delocalized nature of sd-like orbitals, their spin splitting is somewhat smaller than that of the d levels. If we assume the net spin density, arising from the two unpaired spins in the topmost occupied $2t_1\uparrow$ (−0.320) spin orbital, to be delocalized uniformly over four atoms, we find that the spin magneton number per atom in Ni_4 is 0.50.

The main features of the electronic structure of Ni_4 such as the overlapping of d bands by the s band, the passing of the Fermi level through the top of the d bands (where the density of states is high), etc., are very similar to those of Ni_{13},[10] and to the

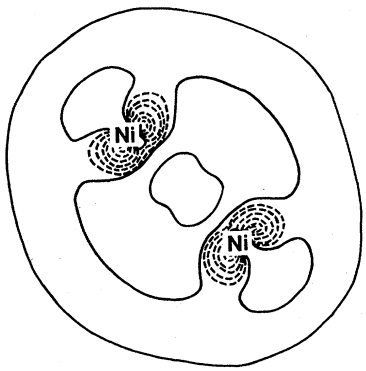

FIG. 7. Contour map for the lowest occupied orbital $1a_1$, if the tetrahedral Ni_4 cluster, plotted in a plane containing two Ni atoms. Contour values decreases in absolute value with decreasing absolute values of the contour labels, the sign of the label giving the sign of the wave function.

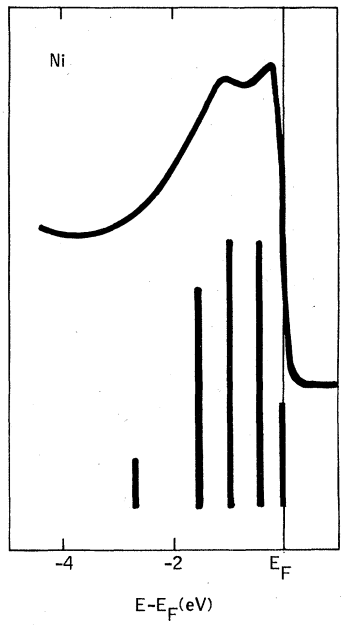

FIG. 8. Comparison of the UPS energy distribution at $h\nu = 21.2$ for Ni with the SCF-$\chi\alpha$-SW calculation for Ni_4. The height of the bars are proportional to the number of occupied electrons. Levels within 0.2 eV are combined.

spin-polarized band structure of ferromagnetic crystalline nickel.[16] Even the spin magneton number (0.5) per atom in paramagnetic Ni_4 is in good agreement with the value (0.54) characteristic of ferromagnetic crystalline nickel.

Figure 8 shows the UPS energy distributions at $h\nu = 21.2$ eV for polycrystalline nickel taken from the work of Eastman[17] and directly underneath the occupied energy levels from the SCF-$X\alpha$-SW spin-restricted calculations for the Ni_4 cluster. The height of the bars is proportional to the number of occupied electrons. Levels within 0.2 eV are combined and appear as a single bar and their energy is determined from the number average of the contributing levels. These results strongly suggest that the four-atom tetrahedral cluster is sufficient to give the principal features of band-structure characteristic of the bulk solid.

In Sec. IV B, we describe the electronic structure of the Ni_3Ti cluster and compare it with that of Ni_4.

B. Ni_3Ti

In going from the Ni_4 cluster to a Ni_3Ti cluster, we replace one Ni atom by a Ti atom and thus reduce the symmetry from Td to C_{3v}. The spin-restricted and the spin-polarized energy levels are displayed on the right-hand side of Figs. 4 and 5, respectively, and labeled according to the irre-

TABLE IV. Energies, occupancies, charge distributions, and fractional principal partial-wave character for the occupied molecular orbitals of a tetrahedral Ni_3Ti cluster, as determined by the spin-polarized SCF-$X\alpha$-SW method. Units and symbols are the same as in Table III. Total Q(Ni)↑: 13.67; total Q(Ti)↑: 10.66; total Q(extra)↑: 0.47; total Q(inter)↑: 1.91; total Q(Ni)↓: 13.50; total Q(Ti)↓: 9.73; total Q(extra)↓: 0.28; total Q(inter)↓: 1.50.

Orbital (occupancy)	Energy	Q(Ni)	(Principal partial-wave components)	Q(Ti)	(Principal partial-wave components)	Q(extra)	(Principal partial-wave components)	Q(inter)
$7a_1$↑(0)	−0.035	4.09×10^{-2}	[0.082(s), 0.842(p), 0.076(d)]	4.75×10^{-2}	[0.163(s), 0.259(p), 0.578(d)]	74.31×10^{-2}	[0.953(s)] [0.023(d)]	8.65×10^{-2}
$7a_1$↓(0)	−0.031	3.85×10^{-2}	[0.089(s), 0.837(p), 0.074(d)]	4.78×10^{-2}	[0.145(s), 0.254(p), 0.602(d)]	75.56×10^{-2}	[0.960(s)] [0.018(d)]	8.11×10^{-2}
$9e$↑(0)	−0.036	5.67×10^{-2}	[0.295(s), 0.639(p), 0.065(d)]	4.94×10^{-2}	[0.031(p), 0.469(d)]	53.02×10^{-2}	[0.971(d)] [0.027(f)]	25.02×10^{-2}
$9e$↓(0)	−0.030	5.58×10^{-2}	[0.298(s), 0.638(p), 0.064(d)]	5.19×10^{-2}	[0.970(d), 0.028(f)]	53.55×10^{-2}	[0.970(d)] [0.028(f)]	24.52×10^{-2}
$6a_1$↑(0)	−0.185	6.19×10^{-2}	[0.463(p), 0.505(d)]	25.61×10^{-2}	[0.194(s), 0.803(d)]	29.66×10^{-2}	[0.975(p)]	26.16×10^{-2}
$6a_1$↓(0)	−0.176	6.06×10^{-2}	[0.466(p), 0.505(d)]	27.67×10^{-2}	[0.170(s), 0.803(d)]	29.12×10^{-2}	[0.973(p)]	25.03×10^{-2}
$8e$↑(0)	−0.208	6.01×10^{-2}	[0.435(s), 0.174(p), 0.392(d)]	39.54×10^{-2}	[0.028(p), 0.972(d)]	23.21×10^{-2}	[0.928(p)] [0.035(f), 0.031(g)]	19.20×10^{-2}
$8e$↓(0)	−0.197	5.46×10^{-2}	[0.421(s), 0.179(p), 0.400(d)]	43.58×10^{-2}	[0.023(p), 0.977(d)]	22.11×10^{-2}	[0.917(p)] [0.043(f), 0.034(g)]	17.95×10^{-2}
$7e$↑(0)	−0.269	6.22×10^{-2}	[0.059(s), 0.047(p), 0.894(d)]	66.54×10^{-2}	[1.000(d)]	3.11×10^{-2}	[0.141(p), 0.528(d)] [0.252(f), 0.079(g)]	11.69×10^{-2}
$7e$↓(0)	−0.255	4.13×10^{-2}	[0.016(s), 0.076(p), 0.908(d)]	71.96×10^{-2}	[1.000(d)]	2.90×10^{-2}	[0.681(d)] [0.193(f), 0.126(g)]	12.77×10^{-2}
$6e$↑(1)	−0.271	15.34×10^{-2}	[0.135(s), 0.070(p), 0.795(d)]	29.42×10^{-2}	[0.996(d)]	9.54×10^{-2}	[0.768(p), 0.061(d)] [0.120(f), 0.051(g)]	15.01×10^{-2}
$6e$↓(0)	−0.263	16.49×10^{-2}	[0.170(s), 0.072(p), 0.758(d)]	22.95×10^{-2}	[0.993(d)]	11.37×10^{-2}	[0.812(p), 0.041(d)] [0.115(f), 0.032(g)]	16.22×10^{-2}
$5a_1$↑(1)	−0.272	4.55×10^{-2}	[0.202(p), 0.785(d)]	54.26×10^{-2}	[0.054(s), 0.945(d)]	8.53×10^{-2}	[0.150(s)] [0.602(p), 0.123(d)]	23.57×10^{-2}
$5a_1$↓(0)	−0.260	$4.ss\times10^{-2}$	[0.244(p), 0.739(d)]	52.74×10^{-2}	[0.060(s), 0.940(d)]	9.53×10^{-2}	[0.151(s)] [0.602(p), 0.115(d)]	25.06×10^{-2}
$2a_2$↑(1)	−0.315	31.80×10^{-2}	[0.992(d)]	0.0		1.62×10^{-2}	[0.870(f)]	2.98×10^{-2}
$2a_2$↓(1)	−0.312	31.81×10^{-2}	[0.992(d)]	0.0		1.61×10^{-2}	[0.869(f)]	2.96×10^{-2}
$5e$↑(2)	−0.341	31.30×10^{-2}	[0.998(d)]	0.85×10^{-2}	[0.029(p), 0.971(d)]	1.16×10^{-2}	[0.034(p), 0.778(d)] [0.039(f), 0.149(g)]	4.11×10^{-2}
$5e$↓(2)	−0.338	31.33×10^{-2}	[0.998(d)]	0.80×10^{-2}	[0.026(p), 0.974(d)]	1.14×10^{-2}	[0.035(p), 0.769(d)] [0.045(f), 0.151(g)]	4.06×10^{-2}
$1a_2$↑(1)	−0.341	32.03×10^{-2}	[1.000(d)]	0.0		0.354×10^{-2}		3.57×10^{-2}
$1a_2$↓(1)	−0.338	32.03×10^{-2}	[1.000(d)]	0.0		0.349×10^{-2}		3.55×10^{-2}
$4e$↑(2)	−0.344	30.37×10^{-2}	[0.014(s), 0.982(d)]	0.09×10^{-2}	[0.601(p), 0.399(d)]	1.60×10^{-2}	[0.537(p), 0.273(d)] [0.068(f), 0.122(g)]	7.21×10^{-2}
$4e$↓(2)	−0.340	30.45×10^{-2}	[0.013(s), 0.982(d)]	0.07×10^{-2}	[0.700(p), 0.300(d)]	1.53×10^{-2}	[0.322(p), 0.280(d)] [0.069(f), 0.129(g)]	7.05×10^{-2}

TABLE IV. (*Continued*)

Orbital (occupancy)	Energy	Q(Ni)	(Principal partial-wave components)	Q(Ti)	(Principal partial-wave components)	Q(extra)	(Principal partial-wave components)	Q(inter)
$3e\uparrow(2)$	−0.374	24.98×10^{-2}	[0.032(s), 0.967(d)	14.46×10^{-2}	[0.011(p), 0.989(d)]	1.56×10^{-2}	[0.246(p), 0.359(d)] [0.234(f), 0.161(g)]	9.03×10^{-2}
$3e\downarrow(2)$	−0.369	25.65×10^{-2}	[0.032(s), 0.967(d)]	12.81×10^{-2}	[0.014(p), 0.986(d)]	1.51×10^{-2}	[0.266(p), 0.344(d)] [0.216(f), 0.173(g)]	8.72×10^{-2}
$4a_1\uparrow(1)$	−0.380	29.77×10^{-2}	[0.998(d)]	1.42×10^{-2}	[0.879(s), 0.082(p), 0.039(d)]	1.42×10^{-2}	[0.236(s)] [0.449(d), 0.230(f)]	7.86×10^{-2}
$4a_1\downarrow(1)$	−0.377	29.78×10^{-2}	[0.999(d)]	1.41×10^{-2}	[0.884(s), 0.086(p), 0.029(d)]	1.41×10^{-2}	[0.255(s)] [0.441(d), 0.220(f)]	7.83×10^{-2}
$2e\uparrow(2)$	−0.387	29.13×10^{-2}	[0.997(d)]	5.12×10^{-2}	[0.029(p), 0.971(d)]	0.76×10^{-2}	[0.134(d)] [0.401(f), 0.458(g)]	6.75×10^{-2}
$2e\downarrow(2)$	−0.383	29.20×10^{-2}	[0.998(d)]	4.76×10^{-2}	[0.033(p), 0.967(d)]	0.77×10^{-2}	[0.142(d)] [0.441(f), 0.416(g)]	6.87×10^{-2}
$3a_1\uparrow(1)$	−0.405	28.58×10^{-2}	[0.984(d)]	2.17×10^{-2}	[0.801(s), 0.128(p), 0.071(d)]	1.42×10^{-2}	[0.538(s)] [0.070(p), 0.296(f)]	10.66×10^{-2}
$3a_1\downarrow(1)$	−0.401	28.61×10^{-2}	[0.983(d)]	2.13×10^{-2}	[0.794(s), 0.132(p), 0.075(d)]	1.43×10^{-2}	[0.554(s)] [0.058(p), 0.294(f)]	10.62×10^{-2}
$1e\uparrow(2)$	−0.412	24.92×10^{-2}	[0.076(s), 0.902(d), 0.020(p)]	10.98×10^{-2}	[0.037(p), 0.963(d)]	1.59×10^{-2}	[0.588(p), 0.117(d)] [0.145(f), 0.149(g)]	12.66×10^{-2}
$1e\downarrow(2)$	−0.407	25.75×10^{-2}	[0.071(s), 0.020(p). 0.909(d)]	9.09×10^{-2}	[0.040(p), 0.960(d)]	1.52×10^{-2}	[0.582(p), 0.123(d)] [0.141(f), 0.154(g)]	12.15×10^{-2}
$2a_1\uparrow(1)$	−0.418	24.52×10^{-2}	[0.960(d)]	7.95×10^{-2}	[0.981(d)]	3.40×10^{-2}	[0.726(s), 0.035(p)] [0.158(f), 0.076(g)]	15.09×10^{-2}
$2a_1\downarrow(1)$	−0.413	24.94×10^{-2}	[0.960(d)]	6.99×10^{-2}	[0.979(d)]	3.31×10^{-2}	[0.723(s), 0.037(p)] [0.158(f), 0.077(g)]	14.87×10^{-2}
$1a_1\uparrow(1)$	−0.502	17.53×10^{-2}	[0.699(s), 0.09(p), 0.208(d)]	7.50×10^{-2}	[0.457(s), 0.142(p), 0.400(d)]	7.22×10^{-2}	[0.929(s)]	32.69×10^{-2}
$1a_1\downarrow(1)$	−0.496	17.70×10^{-2}	[0.693(s), 0.09(p), 0.215(d)]	7.20×10^{-2}	[0.463(s), 0.147(p), 0.390(d)]	7.17×10^{-2}	[0.927(s)]	32.52×10^{-2}

TABLE V. Fractional partial-wave character for the averaged magnetic moment per Ni atom in Ni_4 and Ni_3Ti clusters, as determined by the spin-polarized SCF-$X\alpha$-SW method. Units are in electrons.

	Ni_4	Ni_3Ti
$S(\uparrow)-S(\downarrow)$	−0.01	0.05
$P(\uparrow)-P(\downarrow)$	−0.01	0.02
$D(\uparrow)-D(\downarrow)$	0.51	0.24

ducible representation of C_{3v} point group. The splitting of the energy levels arising from the reduction of symmetry is clearly seen (i.e., $t_2 \rightarrow a_1 + e$ and $t_1 \rightarrow a_2 + e$). The energies, occupancies, charge distributions, and fractional principal partial-wave character of all the occupied orbitals of spin-polarized Ni_3Ti are listed in Table IV. The energies of core levels are also listed with those of Ni_4 in Table II.

We make the following observations.

(i) The occupancy (the density of states) around the "Fermi level" decreases upon alloying.

(ii) In going from Ni_4 to Ni_3Ti, the highest occupied, predominantly d-like and very localized $2t_1$ orbital in Ni_4 splits into $6e$ and $2a_2$ orbitals in Ni_3Ti. The $6e$ orbital is the topmost occupied orbital which is much more spatially delocalized than the $2t_1$ orbital in Ni_4 and contains an appreciable amount of s-like character. The reorganization of charge distribution due to alloying could have important effects on the chemistry of Ni_3Ti and thus its catalytic ability. The orbital contour maps for $2t_1$ in Ni_4 and $6e$ in Ni_3Ti as shown in Figs. 6 and 11, respectively, reveal the differences.

(iii) The width of the d band increases from 0.122 Ry ($1t_2\uparrow$ to $2t_1\downarrow$) to 0.163 Ry ($2a_1\uparrow$ to $4e\downarrow$) in going from Ni_4 to Ni_3Ti.

(iv) Compared to Ni_4, the spin splitting of the energy levels for Ni_3Ti is rather uniform and smaller. It is about the same for both s- and d-like orbitals except the ones near the "Fermi level."

(v) The average magnetic moment per Ni atom decreases in going from Ni_4 to Ni_3Ti. According to the spin-polarized calculation of Ni_3Ti, there are two unpaired spins in the two topmost occupied levels, $6e\uparrow$ (−0.271) and $5a_1\uparrow$ (−0.272). If we assume this net spin to be delocalized uniformly over all four atoms, we find that the spin magnetic number per atom in Ni_3Ti is 0.50, the same as in Ni_4. However, since the orbitals $6e\uparrow$ and $5a_1\uparrow$ are not uniform over the cluster and the local interactions experienced by Ti and by Ni are different, the averaged magnetic moment per Ni atom is different from that per Ti atom. Weighing the

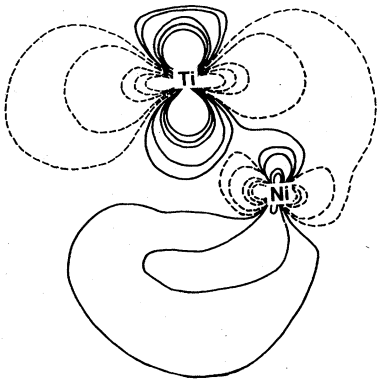

FIG. 10. Contour map for one of the two highest occupied orbital $5a_1$ of the tetrahedral Ni_3Ti cluster, plotted in the plane bisecting the tetrahedron and passing through the Ti atom and one of the Ni atoms.

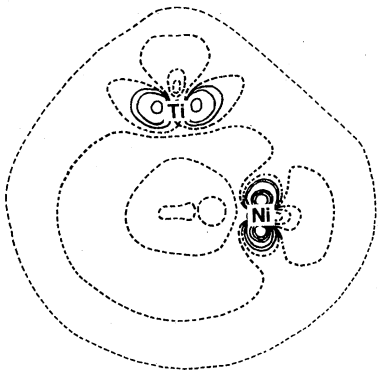

FIG. 9. Contour map for the lowest occupied orbital $1a_1\uparrow$, in the tetrahedral Ni_3Ti cluster, plotted in the plane bisecting the tetrahedron and passing through the Ti atoms and one of the Ni atoms.

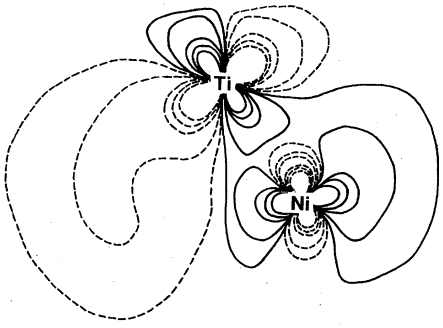

FIG. 11. Contour map for one of the two highest occupied orbital $6e$ of the tetrahedral Ni_3Ti cluster, plotted in the plane bisecting the tetrahedron and passing through the Ti atom and one of the Ni atoms.

contribution of all 34 valence electrons of the cluster to the interatomic region equally, we find that the magnetic moment per Ni atom is equal to $0.31\mu_B$, about $0.19\mu_B$ smaller than that of Ni_4. From the known partial-wave components of the spin orbitals, we can also analyze each partial wave's contribution to the magnetic moment. The results of this analysis for both Ni_4 and Ni_3Ti are summarized in Table V.

(vi) Electronic charge is transferred from Ti to Ni. Using the same weighing scheme in the interatomic region, we can calculate the charge transfer between Ti and Ni. We find that in the process of alloying, there are 0.38 electrons transferred from Ti to each Ni.

In addition to the observations listed above some similarities between Ni_4 and Ni_3Ti are seen to the extent that there is overlap of the d band by the s band and that the bonding character of the orbitals is similar, namely most of the orbitals near the top of the d band are antibonding and nonbonding and most of the orbitals near the bottom of the d band are bonding. The contour maps of orbitals $1a_1\uparrow$, $5a_1\uparrow$, and $6e\uparrow$, plotted in the plane bisecting the tetrahedron and passing through the Ti atom and one of the Ni atoms are shown in Figs. 9, 10, and 11, respectively. It is clearly seen that orbital $1a_1\uparrow$ is bonding and mainly of s-d hybrid character and that $5a_1$ and $6e$ are antibonding and mostly of d character.

V. COMPARISON OF CALCULATIONS WITH MEASURED PROPERTIES OF Ni_3Ti

In this section we shall correlate the theoretical results with the experimental results and the other experimental data available in the literature.

A. Photoemission and the low-temperature electronic specific heat

Figure 12 shows the comparison between the UPS distribution for Ni_3Ti at $h\nu = 21.2$ eV and the simulated density of states from the spin-restricted SCF-$X\alpha$-SW calculation using the procedure described for Fig. 8. We find excellent agreement between calculations and experiment. The most distinctive feature in the UPS distribution, a decrease in electron emission and hence electronic states near the Fermi level, is also observed in the calculation of the prototype Ni_3Ti cluster.

While there is no experimental work on the low-temperature electronic specific heat of the more concentrated Ni-Ti alloys such as Ni_3Ti, there are some on Ni-V systems.[8] The experiment shows that upon alloying V with Ni, the specific heat increases first and then starts dropping when the concentration of V reaches about 12 at.%.

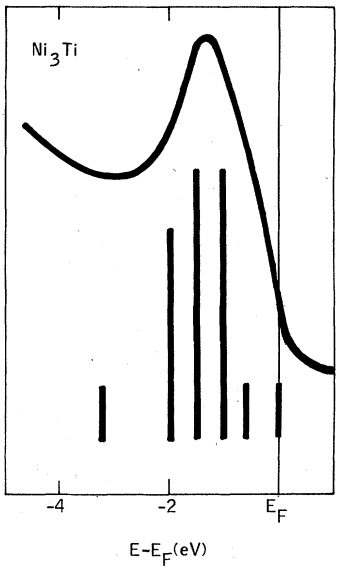

FIG. 12. Comparison of the UPS energy distribution of $h\nu = 21.2$ eV for Ni_3Ti with the SCF-$\chi\alpha$-SW calculation as generated as Fig. 5.

Since V is the closest neighbor of Ti in the first transition period, we expect that the specific heat of Ni-Ti systems to behave the same way. This implies that the density of states at the Fermi level for Ni is higher than that of Ni_3Ti.

B. Auger electron spectroscopy and the x-ray study of core level shifts

Auger electron spectroscopy of Ni and Ni_3Ti obtained by us shows that the relative core level shifts are negligible in going from Ni to Ni_3Ti. From Table II we calculate the energies associated with $K\alpha$, $K\beta$, and $L\alpha$ lines for both Ni_4 and Ni_3Ti. The results, tabulated in Table VI, indeed show that the shifts of inner lines are negligible. Kallne[18] in her x-ray study of the shifts of inner lines of Ti-Ni alloys also shows that the nickel lines shift only a little (~0.5 eV) relative to the pure Ni, which is also consistent with our results.

TABLE VI. The shifts of Ni inner lines of Ni_4 and Ni_3Ti clusters, as calculated by the spin-restricted SCF-$X\alpha$-SW method. Energies are in rydbergs.

	Ni_4	Ni_3Ti
$K\alpha(2P\uparrow-1S\uparrow)$	534.72	534.73
$K\beta(3P\uparrow-1S\uparrow)$	591.35	591.37
$L\alpha(3P\uparrow-2S\uparrow)$	65.50	65.51
$L\alpha(3S\uparrow-2P\uparrow)$	53.92	53.94

C. X-ray emission

Volkov *et al.*[19] in analyzing the x-ray emission L_M bands of Ni, Ni_3Ti, and Ni-Ti alloys showed that the degree of occupation of 3*d* band of Ni in these materials increases in the above order. Using the results tabulated in Tables III and IV and the weighting scheme stated in Sec. IV, we find that the averaged number of *d* electrons per Ni atom in Ni_4 and Ni_3Ti are 9.38 and 9.58, respectively. Since there are five *d* bands and each *d* band can accommodate two electrons per atom, the degree of occupancy of the 3*d* band of Ni increases by about 2% in going from Ni_4 to Ni_3Ti, a trend consistent with the experiment.

D. Mean atomic magnetic moment

Gregory and Moody[8] found that upon alloying Ni with Ti, the mean atomic magnetic moment decreases steadily from $0.616\mu_B$ for Ni to $0.103\mu_B$ for alloy containing 14 at.% of Ti. This is consistent with our theoretical results, namely, that the average magnetic moment per atom associated with Ni decreases from $0.5\mu_B$ for pure Ni to $0.31\mu_B$ for Ni_3Ti. It is interesting to note from Table V that while the mean atomic magnetic moment ($0.5\mu_B$) per Ni atom in Ni_4 essentially comes from the *d*-electron polarization, in the case of Ni_3Ti, because of the effect of the shallower potential of Ti, the charge distribution is reorganized in such a way that on the one hand the magnetic moment decreases and on the other hand the electron polarization involves also *s* electrons.

E. Binding character

Our calculations show a transfer of electronic charge from the titanium to the nickel atoms. This implies that the cohesive bond is no longer purely metallic, but that an ionic component has been added to it. The presence of an ionic (or covalent) component in the bonding of Ni_3Ti is indicated in the phase diagram of the Ni-Ti system[20] by a local maximum of the melting temperature for the composition Ni_3Ti. During the preparation of the samples, we also observed that the compound possesses no ductility. Lack of ductility is a property of ionic or covalent compounds.

F. Work function

Our experiment shows that the work function of Ni_3Ti is less than that of Ni. Our theoretical results presented in Sec. IV also show the same tendency. (i.e., the "Fermi energy" rises in going from Ni_4 to Ni_3Ti.)

VI. CONCLUSION

We have investigated the electronic structure of Ni_3Ti by measuring its photoelectric emission and computing the SCF-$X\alpha$ molecular orbitals of a four-atom Ni_3Ti cluster and a similar Ni_4 cluster which reproduce the local structural and compositional order of the corresponding crystalline alloys. The agreement between the computed and measured electronic structures confirm the earlier finding[10] that computations on such clusters yield an electronic structure that is a resonable representation of that of a bulk material. Since all the atoms of the clusters are effectively "surface atoms," these computations are naturally geared to studies of the surface reactivity and possible catalytic properties of Ni_3Ti alloys. Thus the present work is a first step towards exploring the electronic effect of alloy catalysis.

Our results suggest that the covalent interaction of a Ti atom with neighboring Ni atoms in Ni_3Ti, coupled with the effective charge transfer between Ti and Ni, is sufficiently large that neighboring Ti and Ni sites on the alloy surface cannot be viewed as isolated, unperturbed atoms. Indeed, the Ni sites surrounding a particular Ti site can be viewed as electron-withdrawing "ligands," as in a transition-metal coordination complex, leading to a *formal* valence state of Ti^{3+}. In other words, the Ti site is effectively oxidized by the surrounding Ni sites. However, the actual effective positive charge on a Ti surface site is reduced to ~ +1 by the covalent interaction. This result and the Ni_3Ti electronic structures shown in Figs. 3 and 4, where the occupied part of the *d*-orbital manifold is primarily localized spatially on the Ni sites and the unoccupied part primarily localized on the Ti sites.

ACKNOWLEDGMENT

The research at MIT was supported in part by the National Science Foundation through the Center for Materials Science and Engineering under Grant No. DMR 76-80895.

*Permanent address: Dept. of Physics, National Taiwan University, Taiwan.

[1]Symposium on Ti/Ni and Associated Compounds, J. Appl. Phys. 39, 2166 (1968).

[2]R. J. Wasilewski, S. R. Butler, J. E. Hanlon, and D. Worden, Metall. Trans. 2, 229 (1971).

[3]F. E. Wang and W. J. Buehler, Appl. Phys. Lett. 21, 105 (1972).
[4]L. Brewer and P. R. Wengert, Metall. Trans., 4, 83 (1973).
[5]J. Friedel, Nuovo Cimento Suppl. 7, 287 (1958); P. W. Anderson, Phys. Rev. 124, 41 (1961).
[6]K. H. Johnson, D. D. Vvedensky, and R. P. Messmer, Phys. Rev. B 19, 1519 (1979).
[7]H. Ehrenreich and L. M. Schwartz, Solid State Phys. 31, 150 (1976).
[8]I. P. Gregory and D. E. Moody, J. Phys. F 5, 36 (1975).
[9]E. A. Stern, Phys. Rev. 144, 545 (1966).
[10]R. P. Messmer, S. K. Knudson, K. H. Johnson, J. B. Diamond, and C. Y. Yang, Phys. Rev. 13, 1396 (1976).
[11]J. C. Slater and K. H. Johnson, Phys. Rev. B 5, 844 (1972); K. H. Johnson and F. C. Smith, Jr., *ibid.* 5, 831 (1972).
[12]F. Laver and H. J. Wallbaum, Z. Kristallogr. Kristallgeom. Krystallphys. Kristallchem. A 101, 78 (1939).
[13]P. Duwez and J. H. Taylor, Trans. Metall. Soc. AIME 188, 1173 (1950).
[14]A. Taylor and R. W. Floyd, Acta Crystallogr. 3, 285 (1950).
[15]D. E. Eastman, Solid State Commun. 10, 933 (1972).
[16]J. Callaway and C. S. Wang, Phys. Rev. B 1, 1096 (1973).
[17]D. E. Eastman, J. Appl. Phys. 40, 1387 (1969).
[18]E. Kallne, J. Phys. F 4, 167 (1974).
[19]V. F. Volkov and M. A. Blokhin, Fiz. Met. Metalloved. (USSR) 26, 376 (1968); W. M. Lomor and W. Marshall, Philos. Mag. 3, 185 (1958).
[20]M. Hansen, *Constitution of Binary Alloys* (McGraw-Hill, New York, 1958), p. 1049.